EXTENDED PDF FORMAT
SPONSORED BY
Travel Grants to the 15th International Congress of Immunology Apply Now!
R&D SYSTEMS
www.rndsystems.com

Suppression of Metal-Insulator Transition in VO_2 by Electric Field–Induced Oxygen Vacancy Formation

Jaewoo Jeong *et al.*

Science **339**, 1402 (2013);
DOI: 10.1126/science.1230512

This copy is for your personal, non-commercial use only.

If you wish to distribute this article to others, you can order high-quality copies for your colleagues, clients, or customers by clicking here.

Permission to republish or repurpose articles or portions of articles can be obtained by following the guidelines here.

The following resources related to this article are available online at www.sciencemag.org (this information is current as of April 15, 2013):

Updated information and services, including high-resolution figures, can be found in the online version of this article at:
http://www.sciencemag.org/content/339/6126/1402.full.html

Supporting Online Material can be found at:
http://www.sciencemag.org/content/suppl/2013/03/20/339.6126.1402.DC1.html

This article **cites 29 articles**, 2 of which can be accessed free:
http://www.sciencemag.org/content/339/6126/1402.full.html#ref-list-1

This article appears in the following **subject collections:**
Physics
http://www.sciencemag.org/cgi/collection/physics

Downloaded from www.sciencemag.org on April 15, 2013

Science (print ISSN 0036-8075; online ISSN 1095-9203) is published weekly, except the last week in December, by the American Association for the Advancement of Science, 1200 New York Avenue NW, Washington, DC 20005. Copyright 2013 by the American Association for the Advancement of Science; all rights reserved. The title *Science* is a registered trademark of AAAS.

Suppression of Metal-Insulator Transition in VO_2 by Electric Field–Induced Oxygen Vacancy Formation

Jaewoo Jeong,[1,2] Nagaphani Aetukuri,[1,3] Tanja Graf,[1] Thomas D. Schladt,[1] Mahesh G. Samant,[1] Stuart S. P. Parkin[1]*

Electrolyte gating with ionic liquids is a powerful tool for inducing novel conducting phases in correlated insulators. An archetypal correlated material is vanadium dioxide (VO_2), which is insulating only at temperatures below a characteristic phase transition temperature. We show that electrolyte gating of epitaxial thin films of VO_2 suppresses the metal-to-insulator transition and stabilizes the metallic phase to temperatures below 5 kelvin, even after the ionic liquid is completely removed. We found that electrolyte gating of VO_2 leads not to electrostatically induced carriers but instead to the electric field–induced creation of oxygen vacancies, with consequent migration of oxygen from the oxide film into the ionic liquid. This mechanism should be taken into account in the interpretation of ionic liquid gating experiments.

The electric field–induced metallization of correlated insulators is a powerful means of creating novel electronic phases, but the process requires high electric fields often beyond those achievable by conventional dielectric gates (*1*–*3*). Such fields can be achieved at interfaces with the use of Schottky junctions (*4*) or polar materials (*5*, *6*), or at surfaces with the use of ionic liquids (ILs) (*7*) as the gate dielectric in field-effect transistor devices (*8*–*10*). The latter method allows for tunable electric fields without restriction on the channel material or its crystal orientation. One of the most interesting and widely studied correlated materials is the insulator VO_2 (*11*, *12*), which exhibits a metal-to-insulator phase transition (MIT) as the temperature is reduced below ~340 K in bulk material (*13*). Recently, electrolyte gating (EG) was shown to substantially alter the properties of thin films of VO_2; in particular, the metallization of the insulating state was achieved and attributed to the introduction of small numbers of carriers that are electrostatically induced by the gating process (*14*). This would be consistent with the destabilization of a Mott insulating state in VO_2 that depends critically on electronic band half-filling, which has been a long-standing goal in condensed matter physics (*15*). We find that an entirely different mechanism accounts for the EG suppression of the MIT to low temperatures in epitaxial thin films of VO_2 that we have prepared on TiO_2 and Al_2O_3 single-crystal substrates.

Figure 1A shows resistivity-temperature curves for VO_2 films grown by pulsed laser deposition on various facets of TiO_2 and Al_2O_3 single crystals in an O_2 pressure (P_{O_2}) of 10^{-2} torr during deposition (*16*). The MIT temperature (T_{MIT}) varied as a result of different strains in the VO_2 films (*17*). Henceforth, we focus on films grown on $TiO_2(001)$ and $Al_2O_3(10\bar{1}0)$, which have a large difference in T_{MIT} but have the same crystallographic orientation. For these films, high-resolution x-ray diffraction (Fig. 1B) indicated excellent epitaxial growth with the *c* axis out of the plane. The film on $TiO_2(001)$ is 10 nm thick, is strained along the *c* axis by –1.2% (*18*, *19*), and has a T_{MIT} of ~290 K. By contrast, the film on $Al_2O_3(10\bar{1}0)$ is 20 nm thick, is completely relaxed (*18*, *19*), and has a T_{MIT} of ~340 K.

Devices for EG studies were fabricated from 10-nm $VO_2/TiO_2(001)$ and 20-nm $VO_2/Al_2O_3(10\bar{1}0)$ films (Fig. 1C), unless otherwise noted, using standard optical lithographic techniques. The electrical contacts to the channel included source and drain contacts as well as four side contacts that were used for four-wire resistance and Hall measurements. A ~100-nl droplet of the IL 1-hexyl-3-methylimidazolium bis(trifluoromethylsulfonyl)-imide (HMIM-TFSI) covered the channel and lateral gate electrode. The gate voltage V_G was swept at 5 mV/s and a source drain voltage V_{SD} = 0.1 V was used, except where noted. Hysteresis in the sheet conductance centered about V_G = 0 V was observed for both substrates (Fig. 1, D and E). By sweeping V_G, the device could be reversibly switched between low- and high-conductance states. Once switched to the high-conductance state, the device was stable at V_G = 0 V and maintained its conductance for many days, even when the IL was washed off the device with isopropyl alcohol (fig. S1). We used x-ray photoelectron spectroscopy (XPS) to verify that the IL was completely removed; no spectroscopic signature of the IL was found (fig. S2). This suggests that the gating effect was not electrostatic in

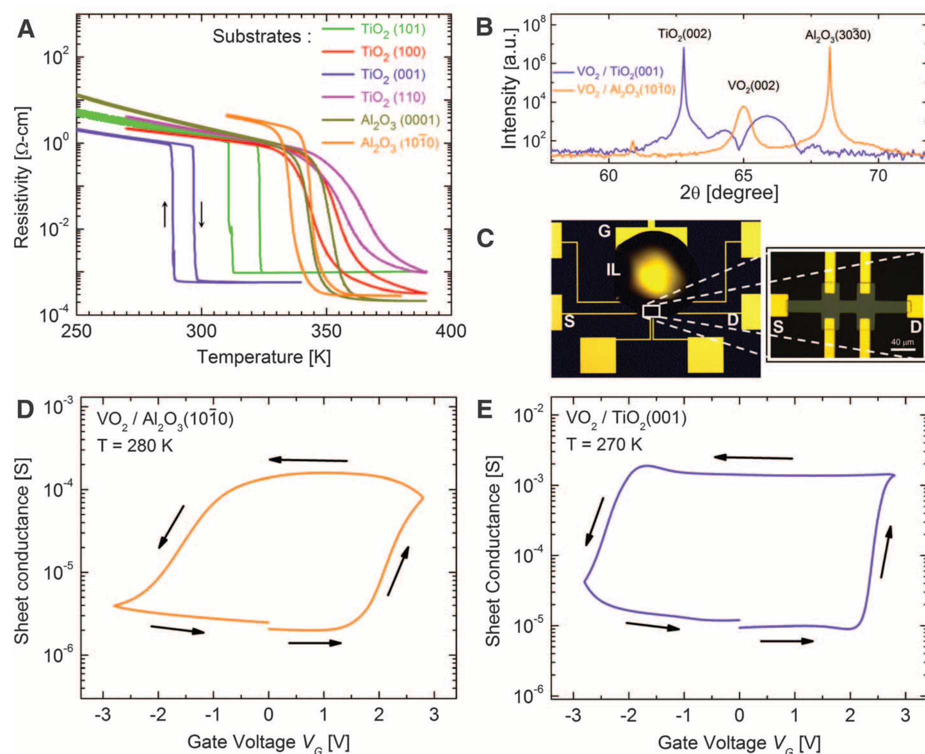

Fig. 1. Temperature- and gate voltage–dependent conductivity of epitaxial VO_2 thin films. (**A**) Resistivity-temperature curves for VO_2 films grown on various orientations of TiO_2 and Al_2O_3 single-crystal substrates. (**B**) High-resolution Cu Kα θ-2θ x-ray diffraction pattern of VO_2 films deposited on $Al_2O_3(10\bar{1}0)$ and $TiO_2(001)$, respectively, showing highly oriented films with the *c* axis out of plane. (**C**) Optical image of a typical device showing a droplet of the ionic liquid (IL) HMIM-TFSI. The electrical contacts can be seen in the magnified image of the channel (right). S, source contact; D, drain contact; G, gate electrode. (**D** and **E**) Sheet conductance versus V_G for devices fabricated from VO_2 films prepared on $Al_2O_3(10\bar{1}0)$ (D) and $TiO_2(001)$ (E).

[1]IBM Almaden Research Center, San Jose, CA 95120, USA. [2]Materials Department, University of California, Santa Barbara, CA 93106, USA. [3]Department of Materials Science and Engineering, Stanford University, Stanford, CA 94305, USA.

*Corresponding author. E-mail: stuart.parkin@us.ibm.com

Downloaded from www.sciencemag.org on April 15, 2013

origin. Moreover, the fact that films on both types of substrates showed similar behavior rules out any appreciable influence of the substrate—for example, the role of strain. The electric field–induced metallic phase, reflected in the source-drain current I_{SD}, was stable over extended periods of time in the presence of the IL at $V_G = 0$ V (fig. S3A) and also for modest V_G, but the insulating phase could be nearly recovered by applying reverse gate voltages similar in value to those needed to induce the metallic phase (Fig. 1, D and E). The insulating phase could also be recovered by annealing in oxygen at modest temperatures (~200°C; fig. S4).

Figure 2A shows the temperature dependence of the channel sheet resistance R_S of $VO_2/TiO_2(001)$ devices for several positive values of V_G. A progressive suppression of the MIT as the gate bias

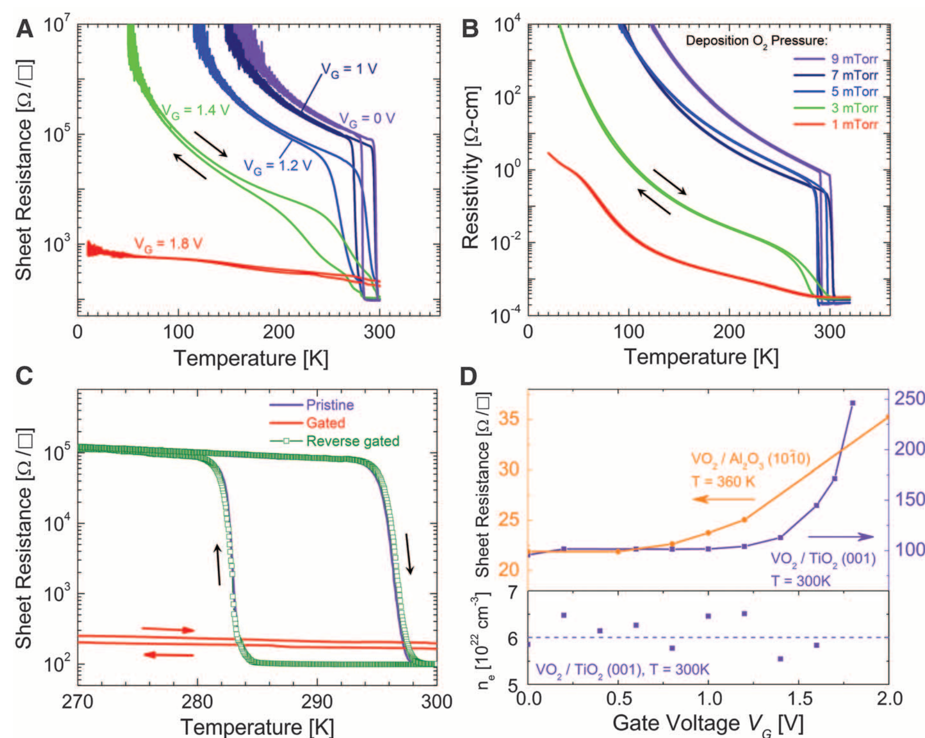

Fig. 2. Suppression of the MIT in VO_2 films. (**A**) Sheet resistance R_s versus temperature T for various gate voltages varying from 0 to 1.8 V for $VO_2/TiO_2(001)$. (**B**) Resistivity of VO_2 versus temperature as a function of P_{O_2} used for film deposition on $TiO_2(001)$. (**C**) R_s versus T for the same device as in (A) in its pristine state, at $V_G = 1.8$ V (gated) and at $V_G = -0.8$ V (reverse gated), showing complete recovery of the MIT in the latter case. V_G was applied at 300 K for measurements in (A) and (C) while the films were in their metallic state. (**D**) Sheet resistance for EG devices formed from $VO_2/TiO_2(001)$ and $VO_2/Al_2O_3(10\bar{1}0)$, and electron carrier density n_e from Hall measurements for an EG device fabricated from $VO_2/TiO_2(001)$, versus V_G. The dashed line is a guide to the eye.

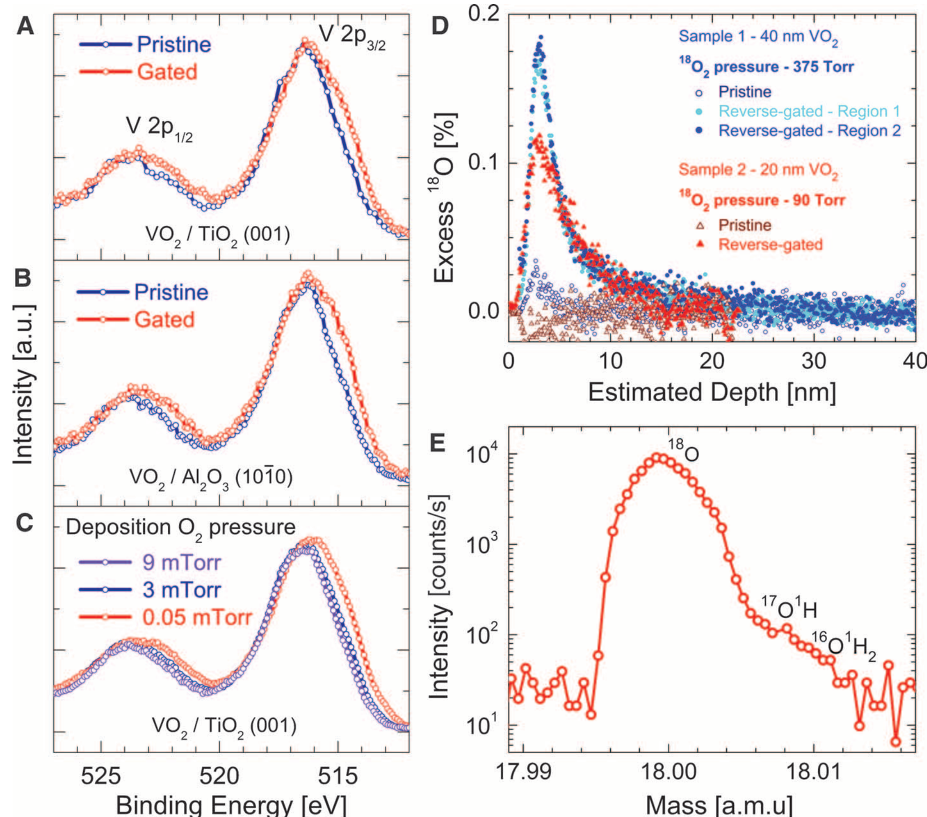

Fig. 3. XPS and SIMS measurements. (**A** and **B**) V 2p core-level spectra for pristine and gated $VO_2/TiO_2(001)$ (A) and $VO_2/Al_2O_3(10\bar{1}0)$ (B); $V_G = 1.8$ V in both cases. (**C**) Comparison of data in (A) and (B) with spectra for VO_2 films deposited under reduced P_{O_2} on $TiO_2(001)$. (**D**) Excess ^{18}O concentration above the natural abundance (~0.2 atomic %) versus depth for two EG devices fabricated from 40- and 20-nm VO_2 on $Al_2O_3(10\bar{1}0)$ determined by SIMS. The devices were gated to the metallic state in vacuum and reverse-gated to recover the insulating state in $^{18}O_2$. Data are compared to pristine channels on the same wafer that were not gated but were subjected to the same dosage of $^{18}O_2$. Measurements on two different areas of sample 1 are very similar. (**E**) Scan at a mass resolution of 4000 (atomic mass units divided by full width at half maximum) showing clear separation of ^{18}O, $^{16}O^1H_2$, and $^{17}O^1H$.

Downloaded from www.sciencemag.org on April 15, 2013

was increased is observed until the MIT is suppressed to below 5 K at $V_G \sim 1.8$ V. This gating effect is compared in Fig. 2B with the effect of changing the oxygen content of VO_2 by depositing $VO_2/TiO_2(001)$ in reduced P_{O_2} at 400°C. The T_{MIT} is systematically reduced and the MIT is suppressed as P_{O_2} is lowered. The transport data in Fig. 2, A and B, are notably similar. In both cases, the onset temperature for the MIT is decreased and the magnitude of the resistivity change drops. The similarity in these data suggests that the EG effect could also be due to the electric field–induced formation of oxygen vacancies, thereby leading to a reduced MIT.

As discussed above, the VO_2 devices can be reversibly switched between insulating and metallic phases. The temperature dependence of the resistivity for the same device in Fig. 2A in its pristine (i.e., ungated) state is nearly identical after being reversibly gated (Fig. 2C).

The sheet resistance in the metallic phase just above the MIT is plotted versus V_G in Fig. 2D for the devices used in Fig. 2A, and for devices on Al_2O_3 substrates in fig. S5. For VO_2 devices on both substrates, R_S increases considerably as V_G is increased. If the gating effect were electrostatic, the electron carrier density n_e should increase for positive V_G; thus, one would anticipate a decrease rather than an increase in R_S. Moreover, Hall resistivity measurements for VO_2/TiO_2 show no evidence for any increase in n_e (Fig. 2D, bottom); rather, n_e is independent of V_G and its measured value is $\sim 6 \times 10^{22}$ cm^{-3}, similar to bulk VO_2 (*20*).

To confirm the possibility of oxygen vacancy creation during EG that was suggested by our transport data, we carried out three independent experimental studies. First, we used XPS to measure changes in the oxidation state of vanadium in gated VO_2 films. Devices with much larger channel areas (~900 by 300 μm) than those used above were fabricated to accommodate the x-ray (Al Kα) beam size (diameter ~150 μm). Transport data for these devices were similar to those shown in Fig. 2 for similar V_G. In Fig. 3, A and B, the V 2p core-level spectra obtained within the channel for pristine devices are compared with the spectra for the same devices gated to completely suppress the MIT to low temperatures. The results for devices fabricated on $Al_2O_3(10\bar{1}0)$ and $TiO_2(001)$ are similar. The position of the V $2p_{3/2}$ core-level peak in the pristine sample is ~516.3 eV, close to the well-established value of ~516.1 eV for V^{4+} in VO_2. In the gated sample (for which the IL was removed), the V $2p_{3/2}$ core-level peak broadens and is shifted toward lower binding energy by ~0.2 eV. (Note that the peak is observed to be at ~515.8 eV for V^{3+} in V_2O_3.) These observations indicate a reduction in the oxidation state of V from V^{4+} toward V^{3+} (*21*). Similarly, in situ measured films prepared at different values of P_{O_2} (Fig. 3C) have V 2p peaks that shift systematically to lower binding energies and broaden monotonically as P_{O_2} is reduced. Thus, the V oxidation state continuously evolves toward V^{3+}, concomitant with a suppression of the MIT (as shown in Fig. 2B).

The changes in the oxidation state of V observed by XPS strongly indicate the formation of oxygen vacancies. In the absence of electric fields, the formation energies of oxygen vacancies in rutile oxides are known to be very high (*22*). However, we hypothesize that the electric fields created at the electric double layer (EDL) at the IL-oxide interface are sufficiently high (*23*) to drive oxygen out of the VO_2 surface into the IL, and that once the oxygen vacancies are created, these vacancies are stable in the absence of the EDL at $V_G = 0$. This explains the nonvolatility of the gating (Fig. 1, D and E). To test this hypothesis, we carried out gating in a high-vacuum chamber in which we could introduce $^{18}O_2$. First, an EG device with a large channel area (900 by 300 μm) was gated in high vacuum ($V_G = 3$ V) to suppress the MIT to low temperatures. After gating for long times (~10 to 20 min), the channel conductance was found to be nearly saturated and remained unchanged when V_G was reduced to zero (*16*). Once a stable channel current was obtained, $^{18}O_2$ was introduced into the chamber at $V_G = 0$ V. Then a reverse gate voltage of –1.5 V was applied until the insulating state was recovered; this took several hours. This procedure was repeated three and four times, respectively, for two experimental devices termed sample 1 and sample 2. Samples 1 and 2 were fabricated from 40-nm and 20-nm $VO_2/Al_2O_3(10\bar{1}0)$, respectively. Depth profile secondary ion mass spectrometry (SIMS) was then performed on these devices after the IL was removed. A comparison was made to pristine regions on the same sample that were otherwise subjected to identical procedures concurrently. In the latter case, no excess ^{18}O above its natural isotopic abundance in oxygen (0.2 atomic percent) was measured. However, a notable increase in the concentration of ^{18}O to nearly twice the natural abundance was found at the surfaces of both devices in the gated channels, with a higher value in sample 1, the device that was gated in higher pressures of $^{18}O_2$ (Fig. 3D). The excess ^{18}O was seen to depths of nearly 20 nm from the oxide surface, with similar depth profiles for the two samples. The incorporation of ^{18}O within the VO_2 channels during reverse gating supports our hypothesis that gating creates oxygen vacancies within the channel.

Given the large area of the channel, the most likely migration path for the oxygen that must be released to create the vacancies during gating is into the IL. Then one might speculate that saturation of the IL with oxygen would prevent such migration. Figure 4A indeed shows that there is no change in the source-drain current even when a large V_G is applied in the presence of O_2 (at 150 torr) to a 100 by 20 μm device of $VO_2/Al_2O_3(10\bar{1}0)$. After 200 s, O_2 was pumped out from the chamber and, concomitantly, I_{SD} gradually increased. When oxygen was reintroduced into the chamber while maintaining V_G = 3 V, I_{SD} began to decrease. We found a clear correlation between the source-drain current and the amount of oxygen in the chamber. A detailed dependence of the sheet conductance on V_G and P_{O_2} is shown in Fig. 4B. Appreciable gating effects were found only at low values of P_{O_2} (for $V_G > \sim 1.5$ V).

Our experiments show that modest gate voltages result in the electric field–induced migration of oxygen into and out of the IL even though the energy required to create an oxygen vacancy in VO_2 in zero electric field is high. This phenomenon is likely to be common to many experiments using high electric fields, especially those using IL gating; many of these experimental results have been interpreted by the electrostatic creation of carriers. Our results suggest that the electric field–induced migration of species into and out of electrolyte-gated materials is an exciting avenue for the creation of novel, non-equilibrium phases of matter.

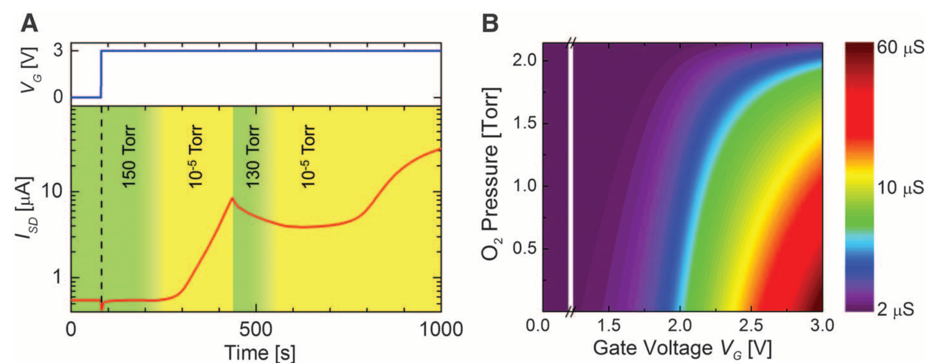

Fig. 4. Electrolyte gating of a device fabricated from $VO_2/Al_2O_3(10\bar{1}0)$ in the presence of oxygen at 300 K. (**A**) Source-drain current at V_G = 3 V versus time as P_{O_2} was varied from an initial pressure of 150 torr, gradually reduced to 10^{-5} torr, abruptly increased to 130 torr, and then gradually reduced to 10^{-5} torr (indicated schematically by color). (**B**) Sheet conductance (color scale) as a function of V_G and P_{O_2}.

References and Notes

1. C. H. Ahn *et al.*, *Rev. Mod. Phys.* **78**, 1185 (2006).
2. A. Cavalleri *et al.*, *Phys. Rev. Lett.* **95**, 067405 (2005).
3. H. Takagi, H. Y. Hwang, *Science* **327**, 1601 (2010).
4. J. Robertson, *J. Vac. Sci. Technol. B* **18**, 1785 (2000).
5. A. Ohtomo, H. Y. Hwang, *Nature* **427**, 423 (2004).
6. P. Moetakef *et al.*, *Appl. Phys. Lett.* **99**, 232116 (2011).
7. M. Galiński, A. Lewandowski, I. Stępniak, *Electrochim. Acta* **51**, 5567 (2006).
8. K. Ueno *et al.*, *Nat. Mater.* **7**, 855 (2008).

Downloaded from www.sciencemag.org on April 15, 2013

9. J. T. Ye *et al.*, *Nat. Mater.* **9**, 125 (2010).
10. Y. Lee *et al.*, *Phys. Rev. Lett.* **106**, 136809 (2011).
11. M. M. Qazilbash *et al.*, *Science* **318**, 1750 (2007).
12. M. Liu *et al.*, *Nature* **487**, 345 (2012).
13. F. J. Morin, *Phys. Rev. Lett.* **3**, 34 (1959).
14. M. Nakano *et al.*, *Nature* **487**, 459 (2012).
15. M. Imada, A. Fujimori, Y. Tokura, *Rev. Mod. Phys.* **70**, 1039 (1998).
16. See supplementary materials on *Science* Online.
17. J. Cao *et al.*, *Nat. Nanotechnol.* **4**, 732 (2009).
18. N. F. Mott, *Metal Insulator Transitions* (Taylor & Francis, New York, ed. 2, 1990).
19. R. Restori, D. Schwarzenbach, J. R. Schneider, *Acta Crystallogr. B* **43**, 251 (1987).
20. W. H. Rosevear, W. Paul, *Phys. Rev. B* **7**, 2109 (1973).
21. G. Silversmit, D. Depla, H. Poelman, G. B. Marin, R. De Gryse, *J. Electron Spectrosc. Relat. Phenom.* **135**, 167 (2004).
22. A. Janotti *et al.*, *Phys. Rev. B* **81**, 085212 (2010).
23. R. Kötz, M. Carlen, *Electrochim. Acta* **45**, 2483 (2000).

Acknowledgments: We thank V. Deline, A. Kellock, T. Topuria, and P. Rice for sample characterization, B. Hughes for help with device fabrication, and K. Martens and A. Pushp for useful discussions. Supported by the Graduate School "Material Science in Mainz" [Deutsche Forschungsgemeinschaft (DFG) GSC 266] (T.G.), the Multidisciplinary University Research Initiative program of the Army Research Office (grant W911-NF-09-1-0398) (J.J.), a Feodor Lynen Research Fellowship from the Alexander von Humboldt Foundation (T.D.S.), and a stipend from DFG (GR4000/1-1) (T.G.).

Supplementary Materials
www.sciencemag.org/cgi/content/full/339/6126/1402/DC1
Materials and Methods
Supplementary Text
Figs. S1 to S8
Table S1
References (*24–31*)

20 September 2012; accepted 24 January 2013
10.1126/science.1230512

Photonic Spin Hall Effect at Metasurfaces

Xiaobo Yin,[1,2] Ziliang Ye,[1] Junsuk Rho,[1] Yuan Wang,[1] Xiang Zhang[1,2]*

The spin Hall effect (SHE) of light is very weak because of the extremely small photon momentum and spin-orbit interaction. Here, we report a strong photonic SHE resulting in a measured large splitting of polarized light at metasurfaces. The rapidly varying phase discontinuities along a metasurface, breaking the axial symmetry of the system, enable the direct observation of large transverse motion of circularly polarized light, even at normal incidence. The strong spin-orbit interaction deviates the polarized light from the trajectory prescribed by the ordinary Fermat principle. Such a strong and broadband photonic SHE may provide a route for exploiting the spin and orbit angular momentum of light for information processing and communication.

The relativistic spin-orbit coupling of electrons results in intrinsic spin precessions and, therefore, spin polarization–dependent transverse currents, leading to the observation of the spin Hall effect (SHE) and the emerging field of spintronics (*1–3*). The coupling between an electron's spin degree of freedom and its orbital motion is similar to the coupling of the transverse electric and magnetic components of a propagating electromagnetic field (*4*). To conserve total angular momentum, an inhomogeneity of material's index of refraction can cause momentum transfer between the orbital and the spin angular momentum of light along its propagation trajectory, resulting in transverse splitting in polarizations. Such a photonic spin Hall effect (PSHE) was recently proposed theoretically to describe the spin-orbit interaction, the geometric phase, and the precession of polarization in weakly inhomogeneous media, as well as the interfaces between homogenous media (*5*, *6*).

However, the experimental observation of the SHE of light is challenging, because the amount of momentum that a photon carries and the spin-orbit interaction between the photon and its medium are exceedingly small. The exploration of such a weak process relies on the accumulation of the effect through many multiple reflections (*7*) or ultrasensitive quantum weak measurements with pre- and postselections of spin states (*8*, *9*). Moreover, the present theory of PSHE assumes the conservation of total angular momentum over the entire beam (*5–9*), which may not hold, especially when tailored wavelength-scale photonic structures are introduced. In this work, we demonstrate experimentally the strong interactions between the spin and the orbital angular momentum of light in a thin metasurface—a two-dimensional (2D) electromagnetic nanostructure with designed in-plane phase retardation at the wavelength scale. In such an optically thin material, the resonance-induced anomalous "skew scattering" of light destroys the axial symmetry of the system that enables us to observe a giant PSHE, even at the normal incidence. In contrast, for interfaces between two homogeneous media, the spin-orbit coupling does not exist at normal incidence (*5–9*).

Metamaterial made of subwavelength composites has electromagnetic responses that largely originate from the designed structures rather than the constituent materials, leading to extraordinary properties including negative index of refraction (*10*, *11*), superlens (*12*), and optical invisibilities (*13*, *14*). As 2D metamaterials, metasurfaces have shown intriguing abilities in manifesting electromagnetic waves (*15*, *16*). Recently, anomalous reflection and refraction at a metasurface has been reported (*17*, *18*), and a variety of applications, such as flat lenses, have been explored (*19–22*). However, the general approach toward metasurfaces neglects the spin degree of freedom of light, which can be substantial in these materials. We show here that the rapidly varying in-plane phase retardation that is dependent on position along the metasurface introduces strong spin-orbit interactions, departing the light trajectory (S) from what is depicted by Fermat principles, $S = S_{\mathrm{Fermat}} + S_{\mathrm{SO}}$ (where S_{SO}

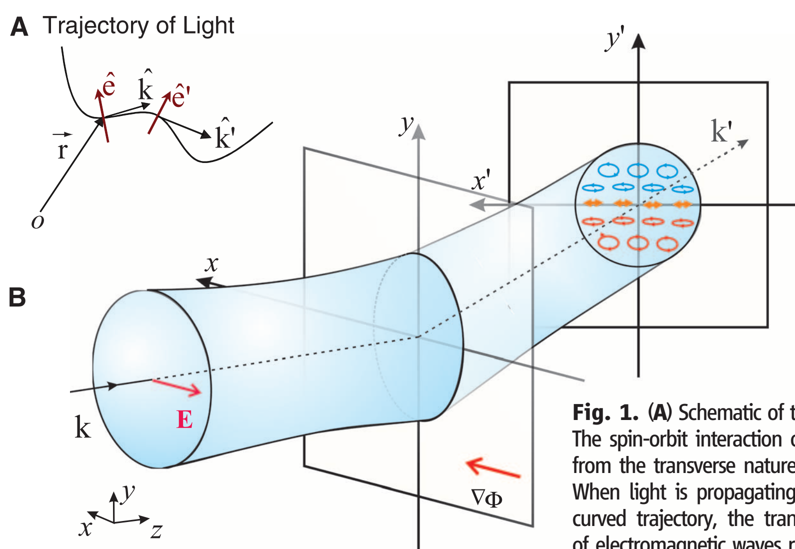

Fig. 1. (**A**) Schematic of the PSHE. The spin-orbit interaction originates from the transverse nature of light. When light is propagating along a curved trajectory, the transversality of electromagnetic waves requires a rotation in polarization. (**B**) Transverse polarization splitting induced by a metasurface with a strong gradient of phase retardation along the x direction. The rapid phase retardation refracts light in a skewing direction and results in the PSHE. The strong spin-orbit interaction within the optically thin material leads to the accumulation of circular components of the beam in the transverse directions (y' directions) of the beam, even when the incident angle is normal to the surface.

[1]National Science Foundation Nanoscale Science and Engineering Center, 3112 Etcheverry Hall, University of California at Berkeley, Berkeley, CA 94720, USA. [2]Materials Sciences Division, Lawrence Berkeley National Laboratory (LBNL), 1 Cyclotron Road, Berkeley, CA 94720, USA.

*Corresponding author. E-mail: xiang@berkeley.edu

Downloaded from www.sciencemag.org on April 15, 2013